New Developments in the Design and Production of Container Assemblies

Prepared by – Volker Wieser, Christof Sommitsch, Kurt Haberfellner, Paul Lehofer
Böhler Edelstahl GmbH & Co KG, Austria

ABSTRACT --- The biggest change in containers during recent years has been the improved temperature control of billet and container. Such containers are equipped with modern resistance heating and helical cooling systems. Practical experience has shown that the advantage of the more uniform temperature distribution has a negative effect on the life of the mantles of such containers. To improve the life of these state-of-the-art containers, the extrusion process in a container for a medium sized press was simulated using the Finite Element Method. The results show the development of temperatures and stresses over a number of extrusions until the process reached an equilibrium. Combining these results with the hot properties of the hot work steels used for the containers allows the prediction of the lifetime of these components. In this paper, the results of the simulation and possible improvements in the design of containers and the most suitable container materials are discussed.

INTRODUCTION

The demand for increased press productivity has led to a trend towards larger and, above all, longer containers. Container lengths of up to 2000 mm (80 in.) are fairly common, especially for the indirect extrusion process. At the same time, an improvement in the quality of the extruded product is desired. The answer is the “Smart Container”, developed by suppliers of extrusion presses and/or tooling .

These containers have an electrical resistance heating system enhanced by a cooling system at the mantle/liner-holder interface (Figure 1).

Figure 1: Shrink-fitting of a liner holder

Depending on the length of the container there are up to 8 heating zones and 4 cooling zones to ensure a maximum temperature deviation of +/- 10°C (18°F) in the liner. This can only be achieved by using an ingenious temperature controller which supplies the data for an advanced PLC [1]. The PLC system controls the heating and the cooling systems and it is quite usual for both modules to be in operation at the same time.

This means that the container mantle is heated from the outside (the heating elements are situated within the mantle or in the container housing) and is cooled from the interface between mantle and liner holder. In other words, the mantle is heated from the outside and cooled from the inside. It is easy to understand that this creates a lot of stress in the mantle. It came out that the life of such a mantle is significantly shorter than that of a mantle of the old-fashioned type without cooling, due to cracks which mainly propagate between the mantle bore and the heating bores (or the keyway on the mantle outer diameter).

To improve the life of these state-of-the-art containers, the extrusion process in a container for a medium sized press was simulated using the Finite Element Method [2]. The results show the development of temperatures and stresses over a number of extrusions until the process reached an equilibrium. Combining these results with the hot properties of the hot work steels used for the containers allows us to predict the life of these

components. The simulation confirmed our practical experience that state-of-the-art containers improve the extrusion process but increase the stresses in the container components.

SIMULATION

For the simulation we chose a highly loaded medium-sized 2-part container with the heating system in the container housing supported by additional heating elements on the faces of the container and a cooling spiral at the mantle/liner interface (Figure 2).

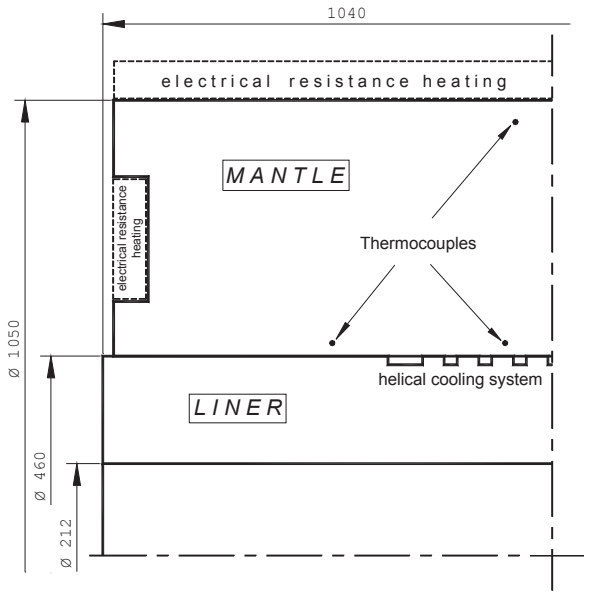

Figure 2: Geometry of the container

The program used, DEFORM™ 2D, offers the possibility of “Multiple Operations” so allowing the simple definition of complex multiple processes. In this case, the shrink-fitting of the liner holder, the pre-heating to working temperature of the container and the process cycles could be defined in one input file. Since the container assembly is symmetrical, an axi-symmetric model of the container was used. In addition, only half of the length was modelled.

The temperature-dependent thermophysical material properties (thermal expansion, thermal conductivity, heat capacity and emissivity) for the liner made of Böhler W300 (H11) and for the mantle made of Böhler W302 (H13) were taken from existing material databases. The necessary contact conditions (friction, interface heat transfer coefficient) between liner and mantel and the boundary conditions (convection coefficient, emissivity) were described using existing data.

Shrink-fitting and heating

The stresses arising during shrink-fitting were calculated in one simulation step for a shrinkage corresponding to 2‰ of the internal diameter of the container. The subsequent heating of the container to temperature took place in 50°C (122°F) steps with a holding time of between 40 min and 1 hour at each temperature step. These holding times are necessary for the temperature to equalise across the thickness of the container. The measuring points (thermocouples) shown in Figure 2 were used to control this process. The total heating time is approx. 30 hours. Figure 3 shows the temperature distribution following heating. The large temperature gradient at the contact surface between liner and mantle and the low temperature of 380°C (716°F) at the abutting face of the liner can clearly be seen. The temperature in the mantle is between 420°C (788°F) and 500 °C (932°F).

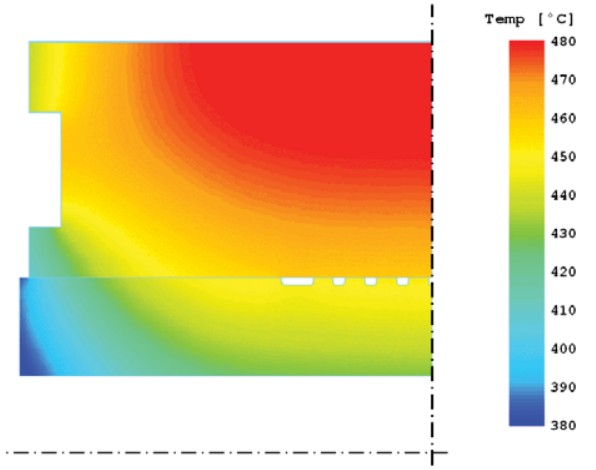

Figure 3: Temperature distribution after heating

The calculated effective stress (Figure 4) is dependent on the degree of shrinkage and the temperature distribution in the container after heating.

In addition, a concentration of the effective stress can clearly be seen at the inside diameter of the liner due to the presence of cooling spiral.

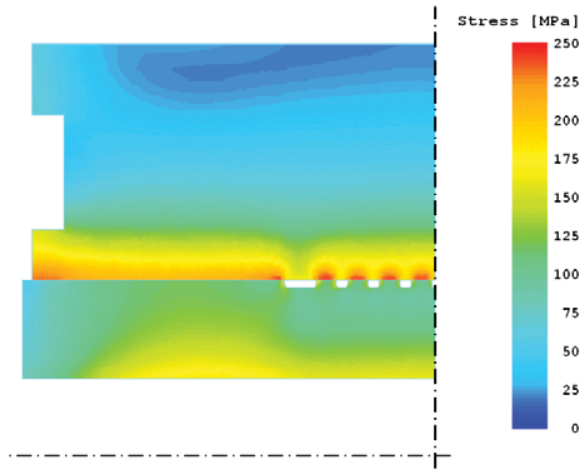

Figure 4: Effective stress following heating.

In contrast, a decrease in effective stress at the free surface between the mantle and the cooling spiral can be observed. At the contact surface the effective stress is approx. 230 MPa (33 ksi).

Extrusion cycle

The loading during an extrusion cycle was defined by an even temperature and a radial compressive stress at the inner diameter of the liner (Figure 5). 35 extrusion cycles were simulated to reach a quasi-stationary operating condition.

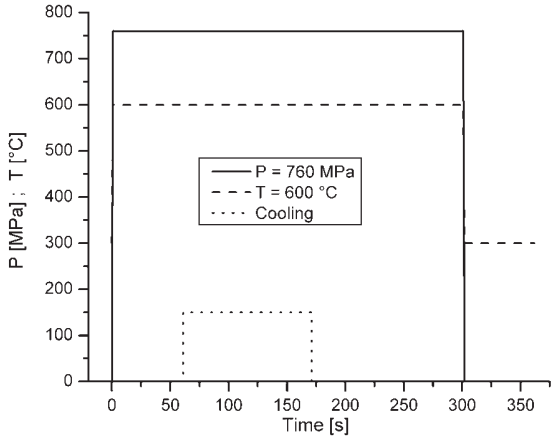

Figure 5: Extrusion cycle (pressure P, temp. T)

A specific pressure of 760 MPa (110 ksi) and a cycle time of 360s, of which 300s was the actual extrusion time, were assumed. Heating and cooling were controlled by the thermocouple positioned as shown in Figure 2.

In this paper we concentrate only on the temperature and stress situation in the mantle occurring in a typical extrusion cycle.
Figs. 6 and 7 show the temperature and stress situation at the beginning of the extrusion cycle. At the inner diameter of the mantle, where the helical cooling system is situated, the stresses increase to approx. 760 MPa (110 ksi). With increasing distance from the helical cooling system the stresses decrease to approx. 570 MPa (83 ksi).

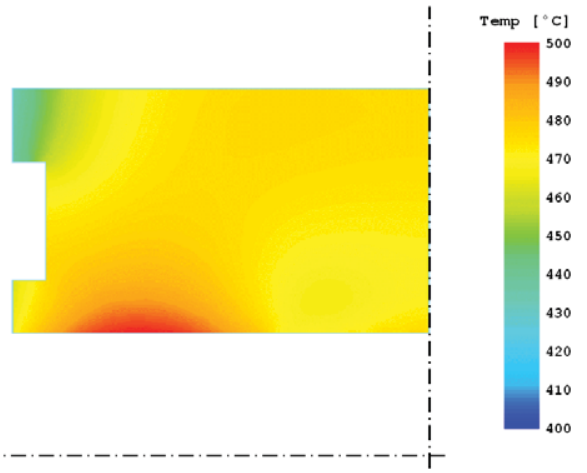

Figure 6: Temperature during an extrusion cycle with no cooling

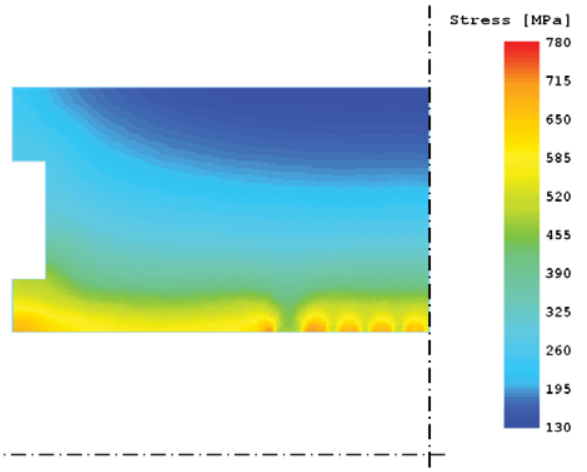

Figure 7: Effective stress during an extrusion cycle with no cooling

If the cooling system (compressed air at approx. 5 bar) is switched on, the temperature in the area near the cooling spirals is reduced from 460°C (860°F) to approx. 385°C (725°F). In this thin layer the temperature differential of 75°C (167°F) results in a significant increase in stress (Figure 9)

and at the given temperatures effective stresses of over 800 MPa (116 ksi) arise.

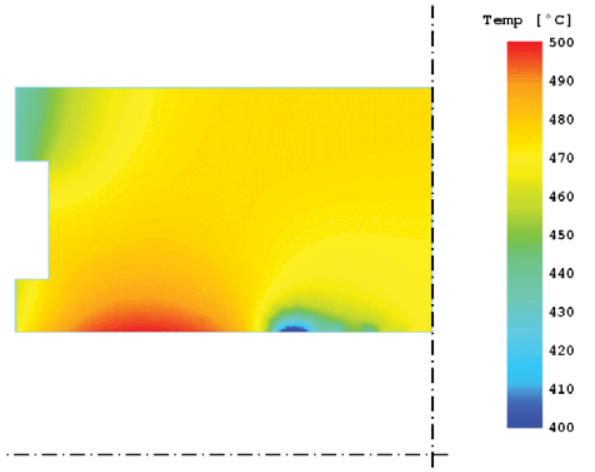

Figure 8: Temperature during an extrusion cycle with cooling

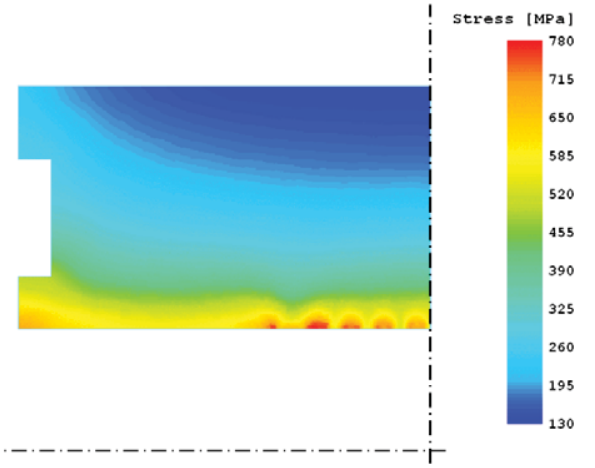

Figure 9: Effective stress during an extrusion cycle with cooling

LIFE TIME PREDICTION IN THE CREEP-FATIGUE INTERACTION REGIME

During the extrusion process, the container and the dies are exposed to high temperatures and are subjected to more or less regularly repeated (i.e. periodical), thermal and/or mechanical loadings. High-temperature damage processes which also occur in stationary loading conditions are ascribed to creep. Others – which appear as a consequence of variations in stress, and are essentially different – belong to fatigue. Due to the typically low number of cycles to failure, the regime of creep-fatigue interaction is often designated as high-temperature low-cycle fatigue. The great variety of possible creep and fatigue damage and failure mechanisms, and above all their interactions, makes a reliable lifetime prediction extremely difficult. Numerous comprehensive investigations have dealt with different aspects of this problem in the last few decades; see e.g. [3-7].

The “Strain Rate Modified” creep model (SRM) is used to predict lifetime. In this approach [6,8] it is assumed that damage accumulates linearly, whereby damage is implicitly defined as (or measured by) exhaustion *D*. The evolution of this is given by

$$D(t) = \int_0^t \dot{D}(t')\,dt' \qquad (1)$$

where the rate of damage, $\dot{D}$, depends on the parameters of loading but not on the actual value of damage itself. The number of cycles to failure under constant cyclic loading with period Δt is then the reciprocal of the damage accumulated in one cycle:

$$N_f = \left(\int_0^{\Delta t} \dot{D}(t)\,dt \right)^{-1} \qquad (2).$$

The deviation from steady-state creep, as the limiting case of high-temperature deformation behaviour, can be measured by the ratio of the inelastic strain rate, $\dot{\varepsilon}_{in}$, at any instant in time, to the rate of steady-state creep, $\dot{\varepsilon}_{sc}$, under the stress applied at that instant:

$$r(t) = \frac{\dot{\varepsilon}_{in}(t)}{\dot{\varepsilon}_{sc}[\sigma(t)]} \qquad (3).$$

Since creep deformation and damage processes are closely related, as are their rates, the same ratio can also quantify the deviation from the rate of damage characteristic for creep, $\dot{D}_C$:

$$\dot{D}_C(t) = \frac{1}{t_{f,c}[\sigma(t)]} \qquad (4),$$

where $t_{f,c}[\sigma(t)]$ is the time to failure in a creep test performed under the actual stress at time t.

The following simple empirical power-law dependence is assumed to be appropriate to define the rate of damage, allowing for the contribution and the interaction of damage mechanisms other than those accompanying steady-state creep deformation, and particularly of fatigue:

$$\dot{D}_{SRM}(t) = |r(t)|^{\nu}\, \dot{D}_C(t) \qquad (5),$$

where ν is an adjustable parameter, and the subscript SRM indicates that the damage rate is defined as the "Strain Rate Modified" rate of creep damage.
After the substitution of (4) into (5), the kinetic law of the evolution of damage reads

$$\dot{D}_{SRM}(t) = \frac{1}{t_{f,c}[\sigma(t)]}|r(t)|^{\nu} \qquad (6).$$

This should be valid for a broader range than just cyclic creep conditions, namely also for the range of creep-fatigue interaction.
From the linearity of the kinetic law of damage evolution it follows that damage D_{SRM} still represents exhaustion. Thus the assumption of the linear accumulation of damage is retained. Substituting (6) into (1), the rule of linear accumulation of Strain Rate Modified Creep damage and the corresponding prediction of cyclic life respectively are obtained. The latter reads explicitly

$$N_{f,SRM} = \left(\int_0^{\Delta t} \frac{1}{t_{f,c}[\sigma(t)]}|r(t)|^{\nu}\, dt \right)^{-1} \qquad (7).$$

Experiments and Calculations

The material properties used in the finite element model were those of the hot work steel grade Böhler W300 (DIN 1.2343). The model parameters ν, $t_{f,c}$ and $\dot{\varepsilon}_{sc}$ were taken from [9]. Six points were chosen along the liner-mantle interface to compare the local damage evolution (Figure 10).

The temperature evolution within one cycle strongly depends on the distance from a cooling spiral. The time dependent local load and temperature give the local stress tensor and thus the von Mises stress (Figure 11).

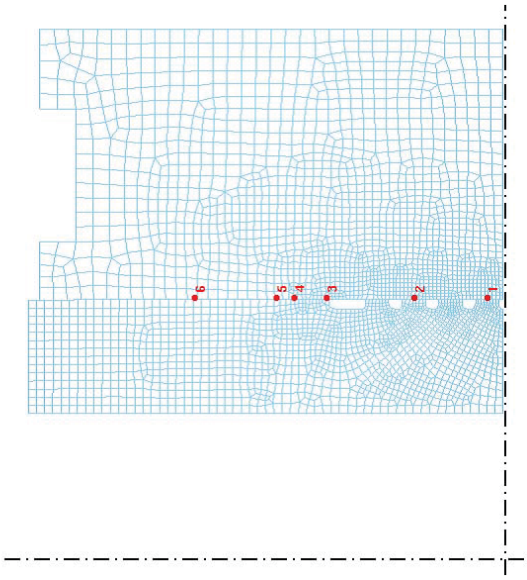

Figure 10: Finite element mesh of the liner-mantle assembly and chosen points at the interface.

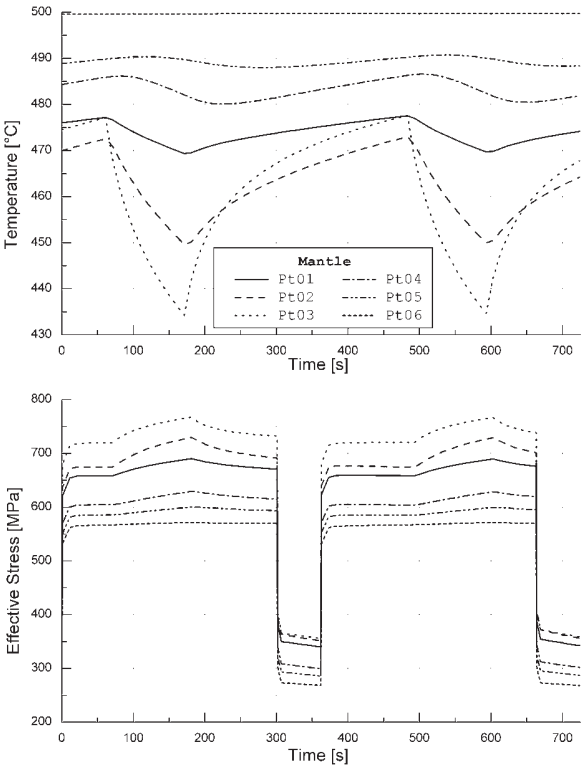

Figure 11: Temperature and effective von Mises stress at six points. Cycle time: 360s, load time: 300s.

To obtain the local inelastic strain rate, cyclic tests were performed for each point. Specimens underwent the effective stress and temperature history of the corresponding points on a thermo-mechanical Gleeble 3800 testing system. The

measurement of strains showed a linear increase with logarithmic time due to inelastic deformation (Figure 12) and hence supplied the local steady state inelastic strain rate $\dot{\varepsilon}_{in}$.

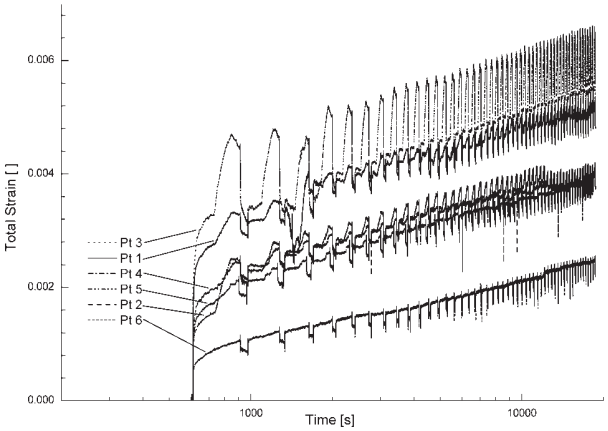

Figure 12: Development of the measured total strain with time for the six points.

Inserting the inelastic strain rates in (7) leads to the number of cycles to failure and lifetime (Table 1). The life time increases with increasing distance from the cooling coil.

Table 1: Inelastic strain rates, number of cycles to failure and lifetime for the six points.

Point number	Inelastic strain rate $x10^{-5}$ [s^{-1}]	Number of cycles to failure	Lifetime [h]
1	9.23	1020	12200
2	9.77	909	10900
3	10.80	803	9630
4	7.81	1270	15300
5	8.12	1340	16100
6	5.75	1760	21200

These values indicate that with decreasing distance from the helical cooling system, the temperature amplitude increases and the mean temperature decreases. Therefore the effective stress during loading reaches the highest values next to the cooling spiral (point 3 in figure 10). However, the temperature and hence the creep rate at relatively greater distances to the cooling spiral (point 6 in figure 10) is not high enough to compensate for this. From that the question arises to what extent the cooling could be lowered that the relatively higher creep damage far from the cooling spiral equals the higher fatigue damage near the cooling spiral. Thus, the cooling configuration and cooling process have to consider the whole container assembly, materials properties and process conditions to find an optimum in terms of container life time by calculations.

CONCLUSION

The thermomechanical loading during extrusion means that the container is in a complex state of stress with many interacting forces. The magnitude of both thermal and mechanical loading on the container during extrusion is at the upper limit of that which standard hot work tool steels are intended to withstand. This means that the working life of the liner and therefore the container assembly are shortened [10].

An optimum design of the container can therefore be achieved using the following concepts – in general together, rather than alone.

* Zoned heating and cooling systems can be used in the container in order to keep the temperature of the container as independent as possible from the stress intensity of the extrusion cycle.
* Minimization of the difference between billet temperature and container temperature.
* Use of an ideal combination of materials for the liner and mantle, taking into consideration the thermomechanical loading which occurs during service.
* Axial billet temperature profile
* Press speed as a function of time

FEM, together with the relevant materials science, allows the working life of extruder containers under real-life conditions to be predicted. By varying individual parameters, an optimised extruder container can be designed.

Finally it should be noted that the amount of work involved in gathering data and calculating the necessary parameters for the lifetime prediction is significant.

REFERENCES

1. Eckenbach, Wolfgang, “Temperaturgeführte Blockaufnehmer in Strangpressen,” *Aluminium*, 73, 1997.

2. Robbins, Paul, “Superextruders: Improving Container Life Though Temperature Control,” *Light Metal Age*, April 2003, 44 – 47.

3. Lemaitre, J., *A Course on Damage Mechanics*, Springer, Berlin, Germany, 1996.

4. Sermage, J., Lemaitre, J. and R. Desmorat, Fatigue Fract. Engng. Mater. Struct. 23, 2000, 241-252.

5. Chaboche, J., International Journal of Plasticity 5, 1989, 247-302.

6. Rubesa, D. and R. Danzer, Zeitschrift für Metallkunde. 86, 1995, 832 - 838.

7. Inoue, T., Ohno, N., Suzuki A. and T. Igari, Nuclear Engineering and Design 114, 1989, 295 - 309.

8. Rubesa, D., “Lifetime prediction and constitutive modelling for creep-fatigue interaction,” *Materialkundlich-Technische Reihe 13*, G. Petzow and F. Jeglitsch (Eds.), Gebrueder Borntraeger, Berlin, Germany, 1996, 95 - 98.

9. Mitter, W., Haberfellner, K., Danzer, R. and C. Stickler: *HTM 52*, 1997, 253 - 258.

10. Bauser, Martin and Günther Sauer, Strangpressen, Aluminium-Verlag Düsseldorf, 2001, 2. Auflage